Molecular Dynamics Simulations of Nanocomposites Based on Poly(ϵ-caprolactone) Grafted on Montmorillonite Clay

Fabrice Gardebien,*,† Jean-Luc Brédas,†,‡ and Roberto Lazzaroni†

Service de Chimie des Matériaux Nouveaux, Université de Mons-Hainaut, 20 Place du Parc, B-7000 Mons, Belgium, and School of Chemistry and Biochemistry, Georgia Institute of Technology, Atlanta, Georgia 30332-0400

Received: October 26, 2004; In Final Form: March 21, 2005

Intercalated and exfoliated models of polymer nanocomposites based on poly(ϵ-caprolactone) and functionalized montmorillonite clay are studied by means of molecular dynamics simulations. Intercalated and exfoliated models are considered for probing the structural characteristics of the corresponding nanocomposites prepared by melt intercalation and in situ polymerization, respectively. In the exfoliated system, the organization of the polymer chains onto the clay surface is examined in terms of the density profiles and the order parameter function. A layered structure can clearly be seen to form near the surface with density maxima higher than in amorphous poly(ϵ-caprolactone). This can be viewed as an increase in effective particle thickness, which can contribute to the outstanding gas barrier properties of the exfoliated nanocomposites. The comparison of the structures and energetics of the intercalated model with those of a nanocomposite model based on a nonfunctionalized clay indicates nearly similar characteristics. Nevertheless, the slight differences observed for the interfacial polymer density and clay− and surfactant−polymer binding energies can account for the differences in rheological measurements. The results also suggest that the difference in morphology obtained for the nanocomposites prepared by the two synthetic approaches can be ascribed to both a difference in interfacial polymer density and the formation of bridging polymer chain structures that hinder the exfoliation process.

1. Introduction

Polymer nanocomposites (PNCs) are currently receiving considerable attention because of the remarkable barrier, thermal, and mechanical properties that they exhibit with respect to conventional microcomposites.[1] PNCs consist of clay particles dispersed in a polymer matrix at the nanometer level. The most effective strategy for promoting the dispersion of the clay particles is to increase their miscibility with the polymer matrix by using clays whose natural cations have been exchanged with ionic surfactant molecules. When dispersion is achieved, two extreme structures can be observed as illustrated in Figure 1: (i) an intercalated structure, where the polymer chains are inserted into the interlayer spaces, or galleries, between stacked clay layers and (ii) an exfoliated or delaminated structure, where all individual clay layers are fully separated from each other and are evenly distributed throughout the polymer matrix. For a given polymer, either one of these structures or a hybrid structure where both intercalated and exfoliated domains coexist can be obtained. The phase behavior of the system is strongly dependent on the chosen organo-modified clay as well as on the preparation method.

The structure and dynamics of polymer chains at interfaces have been extensively studied using both molecular dynamics (MD)[2−12] and Monte Carlo simulations.[13−18] The results gathered from these theoretical studies provide limited insight into, for example, the factors that control the intercalation of the polymer chains in the gallery, the role played by the surfactant molecules, or the factors that contribute to the complete dispersion of the sheets. A mean field lattice approach developed by Vaia et al.[19,20] for a system consisting of polymer chains and surfactant chains tethered to silica surfaces has provided a qualitative overview of the conditions that promote intercalation and exfoliation. Another important contribution to the understanding of the phase behavior of this class of materials has stemmed from the work of Balazs and co-workers.[21−24] These authors used a self-consistent-field approach to calculate the free energy of the PNC models: all segment−segment interactions are replaced by the interaction between a segment and the average field created by the other segments. By systematically varying parameters such as the grafting density, the length of the polymer or surfactant chains, and the polymer structure or its interaction parameters, the authors derived useful criteria

Figure 1. Schematic illustration of the two extreme morphologies observed for PNCs termed (a) intercalated and (b) exfoliated.

* To whom correspondence may be addressed. E-mail: fabrice@averell.umh.ac.be. Fax: ++32-65-37-38-61.
† Université de Mons-Hainaut.
‡ Georgia Institute of Technology.

10.1021/jp045122i CCC: $30.25
Published on Web 05/04/2005

for favoring phase miscibility and promoting intercalation or exfoliation. Lee et al.[25−27] have studied the intercalation process by using a model consisting of connected beads for the polymer chains. Their results indicate that the polymer−surface interactions indeed favor intercalation; however, kinetic effects can impede the penetration of the polymer when these interactions become too strong. More specifically, PNCs based on polystyrene[28,29] and poly(ethylene oxide) (PEO)[30−32] have been the topics of combined MD and NMR studies that showed large inhomogeneities in the polymer dynamical behavior across the clay gallery and over a wide range of temperature;[31] confined PEO appears to be more disordered than its bulk amorphous counterpart. The interlayer structure of organo-modified clays has also been investigated using MD techniques in combination with united atom models.[33,34] However, it should be noted that chain conformations at the interface may not be well reproduced with such united atom models, as stated earlier in comparative studies with explicit atom models.[10,15,16]

In this work, we have used atomistic molecular simulation techniques to study nanocomposites based on the biodegradable and biocompatible polymer poly(ϵ-caprolactone) (PCL) and an organo-modified montmorillonite (mmt) clay. Experimentally, the preparation of the PCL nanocomposites, using a mmt modified by the functionalized surfactant methyl bis(2-hydroxyethyl) (tallow alkyl) ammonium (Cloisite 30B), leads to either mixed intercalated−exfoliated or fully exfoliated nanocomposites, depending on the synthetic route (i.e., melt intercalation or in situ polymerization, respectively[35,36]). Furthermore, in the preparation of PCL−Cloisite 30B nanocomposites by in situ polymerization method, the polymer chains are tethered onto the mmt surfaces as a result of prior esterification reactions of the ϵ-caprolactone monomers with the hydroxyl groups of the surfactants.[35] It was also established that both hydroxyl groups of all of the surfactants are growing sites for the PCL chains.[37] Here, the exfoliated PCL nanocomposite, as obtained by in situ polymerization using the mmt Cloisite 30B, has been modeled by taking the above experimental findings into account. MD simulations have been carried out to probe the structure of the polymer chains on the mmt surface. In the synthesis of the PCL−Cloisite 30B nanocomposites, the reasons why different preparation routes lead to different types of morphology (mixed intercalated−exfoliated vs exfoliated) remain unclear; therefore, our goal is also to understand the factors that could explain these different behaviors. To this end, we have undertaken the simulations of a model for the intercalated PCL−Cloisite 30B nanocomposite structure as obtained by melt intercalation. The structural and energetic characteristics of this system were derived and compared to both those of the exfoliated model and those taken from our previous study dealing with the intercalated PCL−Cloisite 25A nanocomposite.[38] Note that in the intercalated cases the polymer chains are not grafted to the surfactant molecules but are simply mixed with them.

The paper is organized as follows: section 2 presents our models for the exfoliated and intercalated PCL−Cloisite 30B nanocomposites. The details of the simulation procedure are also provided. The results are presented in section 3: first, we discuss the results of the simulations on the exfoliated PCL−Cloisite 30B nanocomposite model; then, with a view toward analyzing the factors that control the dispersion of the platelets in the PCL matrix, we present a comparative study between the two models of the PCL−Cloisite 30B nanocomposite (exfoliated and intercalated models) and the intercalated PCL−Cloisite 25A nanocomposite model.

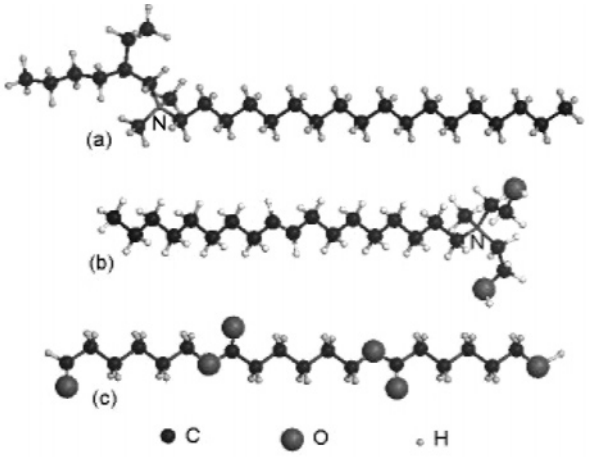

Figure 2. Molecular structures of (a) the dimethyl 2-ethylhexyl *n*-octadecylammonium ion; (b) the methyl bis(2-hydroxyethyl) *n*-octadecenylammonium ion, which correspond to the main organic modifier in Cloisite 25A and Cloisite 30B, respectively; and (c) a three-unit-long PCL chain.

2. Methodology

2.1. Simulation Cells and Models for the Nanocomposites. Montmorillonite is an aluminosilicate made up of one aluminate octahedral sheet sandwiched between two silicate tetrahedral sheets. Isomorphous substitution of metal ions in the crystal lattice by cations of lower charge causes a net permanent negative charge that is balanced by cations in the interlayer space. The model chosen for the montmorillonite clay has been taken from the work of Skipper et al.[39] The clay platelet has *x* and *y* dimensions of 31.7 Å by 18.3 Å, respectively, and bears a negative charge of 9 *e*, which results from the substitutions of Si atoms by Al atoms and Al atoms in octahedral positions by Mg atoms.

In the *exfoliated* model of the PCL−Cloisite 30B nanocomposite, the third dimension of the simulation box has been enlarged up to 150 Å so as to preclude any significant interaction between the adsorbed molecular organic phase and the periodic image of the mmt layer. The organic phase consists of four "macromolecules". Each of these macromolecules is made up of two PCL octamers and a dihydroxyl-bearing alkylammonium surfactant (vide infra): the two octamers are bound to the surfactant by an ester bridge. It should be noted that the bonds created between the surfactant and the two polymer chains exactly correspond to the situation encountered in the preparation of this nanocomposite by in situ polymerization.[35,37]

In our previous study, the surfactant used was the predominant organic modifier of Cloisite 25A.[38] In the present study, the predominant modifier of Cloisite 30B is used. Figure 2 shows the structures of the two surfactants dimethyl 2-ethylhexyl *n*-octadecylammonium and methyl bis(2-hydroxyethyl) *n*-octadecenylammonium, the main modifiers of Cloisite 25A and Cloisite 30B, respectively, along with the structure of a short PCL chain. Structural differences can be observed between the two surfactants. First, the surfactants of Cloisite 30B and Cloisite 25A differ in the structures of two groups bound to the nitrogen atom: two hydroxyethyl groups in the former case and alkyl groups in the latter. Second, the long hydrophobic tail of the surfactant contains a CC double bond only in the case of Cloisite 30B. (Because no information is available on the actual position of this double bond, the middle of the tail has been arbitrarily chosen here.) In the simulation cell, five Na^+ counterions were also added and positioned on the other surface of the mmt layer to ensure electroneutrality.

TABLE 1: Atomic Charges (in atomic units *e*) for Selected Atoms of the Dihydroxyl-Bearing Alkylammonium Surfactant (see Appendix)

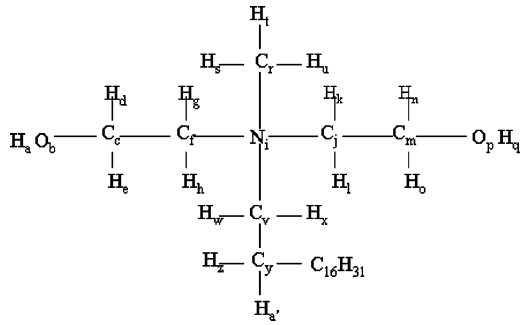

atom index	a	b	c	d	e	f	g	h	i
charge	0.45	−0.71	0.35	0.02	−0.05	−0.05	0.07	0.13	0.05
atom index	j	k	l	m	n	o	p	q	r
charge	0.05	0.10	0.08	0.35	0.00	−0.04	−0.69	0.45	−0.31
atom index	s	t	u	v	w	x	y	z	a′
charge	0.18	0.13	0.15	−0.08	0.10	0.14	−0.03	0.04	0.04

The simulation cell for the *intercalated* PCL−Cloisite 30B nanocomposite was constructed according to the procedure we previously described.[38] The total interlayer density of the organic phase has been chosen on the basis of the requirement that the density in the gallery should be equal to the density of the bulk amorphous polymer. Because the amorphous bulk density of PCL is estimated to be 1.04 g·cm^{-3} by our calculation method, an interlayer total organic density close to this value has been chosen, 1.02 g·cm^{-3}, which corresponds to the insertion of four octamers in the gallery of the model for the PCL−Cloisite 30B nanocomposite. This value is very close to the density chosen (1.03 g·cm^{-3}) for one of the models in the study of the PCL−Cloisite 25A nanocomposite.[38] Furthermore, nine hydroxyl-bearing surfactants are present in the gallery to ensure neutrality. Finally, the interlayer distance was chosen according to experimental data for this nanocomposite, 30 Å.[36]

2.2. Simulation Details. The calculations were performed within the Cerius^2 modeling environment.[40] The Universal Force Field (UFF)[41] has been used in combination with charges for individual surfactant and polymer chains (Table 1) that derive from their electrostatic potential calculated at the HF/6-31G(d) level of theory (CHELPG method[42] as implemented in the Gaussian 98 package[43]). Such sets of charges are known to provide a more realistic description of the charge distribution, compared to the more commonly used charge equilibration method[44] or Mulliken population analysis. Our calculation method was previously validated for the simulation of PCL.[38] For the exfoliated model, we used a less straightforward procedure for charge determination. For this model, the charges of the "surfactant−(PCL octamer)$_2$ macromolecules" have been calculated separately for the subunits (surfactant and octamer); then, the charges at the two junctions between the surfactant and the PCL chains were slightly modified to match those of an ester function in the inner part of an octamer. For large molecular systems, a convenient approach indeed consists in calculating the charges for subunits of more tractable size.[45] For all of the simulations, the charges on all atoms were kept fixed. The Ewald summation method[46] was used for the treatment of the electrostatic interactions. For the van der Waals interactions, the Lennard-Jones potential was driven smoothly to zero for distances between 8.0 and 8.5 Å. Three-dimensional periodic boundary conditions were imposed to avoid boundary artifacts. All simulations were performed in the *NVT* ensemble and were coupled to a Nosé−Hoover thermostat[47−49] to maintain the temperature. The positions of the atoms of the clay were also maintained in fixed positions throughout all simulations.

2.3. Procedure for Generating the Initial Configurations. The initial geometry for the exfoliated PCL−Cloisite 30B model consists of four of the macromolecule described above, positioned on a mmt layer. To fit all four macromolecules on the surface, the three long chains (octadecenyl tail and the two PCL octamers) of each macromolecule were chosen in their all-trans conformation and oriented in a direction roughly perpendicular to the surface. A MD simulation was then performed for 250 ps at 800 K using a force field properly modified to sample efficiently the conformation space of the organic phase. For this simulation, we selected the Dreiding force field instead of UFF to impose relevant modifications of its bonded and nonbonded parameters (because the UFF force field uses a set of functional forms to generate its parameters). The Dreiding force field was modified as follows: (i) the torsional barrier height k_{cc} around all CC bonds was set to zero; (ii) the van der Waals and electrostatic 1−4 interactions were excluded from the total potential energy; and (iii) in the 12−6 Lennard-Jones expression, the ϵ_H parameter was scaled down to favor configurational changes by decreasing the intermolecular interactions.

From the generated set of configurations, we then extracted four configurations according to two criteria related to their potential energy: the configurations were selected on the basis of both the lowest nonbonded energy and the lowest possible total torsional energy. The bond and angle energetic contributions were discarded from the selection criteria for two reasons. First, their large contributions to the potential energy may bias the selection toward, for example, configurations corresponding to high nonbonded energy terms and accidentally low bond and angle potential terms. Second, the successive values of the bond and angle energy contributions cannot be directly related to the configuration changes of the whole organic phase. Once these four configurations were extracted, all further calculation steps described below used the UFF force field. For three of these configurations, an annealing cycle was run over a period of 140 ps from 1500 to 300 K, followed by a 500-ps MD run at 300 K. A second series of simulations started from the fourth configuration, for which an annealing cycle was carried out from 1500 to 600 K over a 95-ps period, followed by a 500-ps MD simulation at 600 K; three other configurations were then selected from this 500-ps simulation according to the same selection criteria presented above; finally, each of these three configurations was cooled to 300 K, and a 500-ps MD run was performed. The diffusion coefficients calculated in the direction normal to the clay layer for the oxygen atoms of the polymer chains are about 0.5×10^{-5} cm^2/s for the explorative MD calculation at 600 K and reach values as high as 10^{-4} cm^2/s for the simulated annealing cycles at 1500 K. The values of these diffusion coefficients reveal massive changes of atom positions during the high-temperature simulations (long simulation at 600 K and annealing from 1500 K). During these simulations, the chains thus acquire sufficient mobility to allow the sampling of a large portion of the potential energy surface and the generation of independent configurations as the temperature of the system is slowly decreased.

By the end of these two series of simulations, one configuration of lowest mean potential energy was used for a further annealing cycle at 1500 K (over a 295-ps period with the temperature decreasing by steps of 30 K in the 700−340 K range), followed by a 500-ps simulation at 300 K. The mean potential energy that was derived after the equilibration period

of that run was very similar to the lowest mean potential energies found in the previous series.

The procedure for generating the configurations for the intercalated PCL−Cloisite 30B nanocomposite model is the same as that extensively described in our previous study for the PCL−Cloisite 25A case.[38] Following the generation procedure, three starting configurations were selected, and in each case, a MD simulation was carried out for 500 ps at 300 K.

For our nanocomposite systems made up of octamers, an estimation of the longest relaxation time using the Rouse model indicates that at least 3 ns of simulation would be necessary. (In this model, the longest relaxation time is proportional to the square of the chain length, N^2, where N stands for the number of beads, which can be taken as 7 in the caprolactone monomer.) Such a time period is prohibitively costly using atomistic models. To overcome this problem, the strategy was to derive many statistically independent configurations that are thermally equilibrated for both the intercalated and exfoliated nanocomposites. Then we analyzed the structural and energetic properties by averaging over the configurations of lowest potential energies arising from all of the 500-ps simulation series. A few hundred picoseconds was used for the data analysis, and for this period, we ensured that the configurations were thermally equilibrated by monitoring the potential energy, temperature, and nonbonded energy variations. In dense systems of long chains, prior to the simulations at 300 K that correspond to very slow chain dynamics, we used high-temperature simulations because these (i) allow the exploration of the phase space (to obtain independent configurations) and (ii) increase the chain motions (this actually reduces the time period required for the subsequent thermal equilibration at 300 K). Two remarks should be added. First, anyone interested in a complete study of the relaxation of the individual chains in the cell with respect to the starting configurations (i.e., prior to any high-temperature simulations) must take into account all the MD trajectories calculated between 1500 and 300 K because most of the dynamics occur at high temperatures. Second, it should also be pointed out that the use of series of a few hundred picosecond simulations at 300 K only cannot allow the relaxation of the chains within a reasonable computational time (at 300 K, the configuration obtained even after 500 ps of simulations is highly correlated with the first at 0 ps).

The calculations of the binding energies between the three subsystems (polymer, surfactant, and mmt), as discussed in section 3.2, were done for structures minimized with a root-mean-square convergence $\lesssim$0.004 kcal/mol/Å for the energy gradient. The binding energy values result from averages taken over the three configurations of the PCL−Cloisite 30B model as they have similar total potential energies. The partial density profiles presented in the comparative study in section 3.2 were derived in each case (the three models based on Cloisite 30B and Cloisite 25A, respectively) using averages made over three configurations. To avoid spiky partial density profiles, the bin sizes have been enlarged to ~0.5 Å in the three cases.

3. Results and Discussion

3.1. Exfoliated Nanocomposite Model. A snapshot from the simulations is shown in Figure 3. As expected, all of the charged heads of the surfactants remain stuck to the surface throughout the simulations while their C_{18} hydrophobic tails are either adsorbed on the surface or extended away from the surface. As in the previous study of the intercalated PCL−Cloisite 25A nanocomposite, the sites of the polymer chains prone to adsorb on the surface are the ester functions and the methylene groups

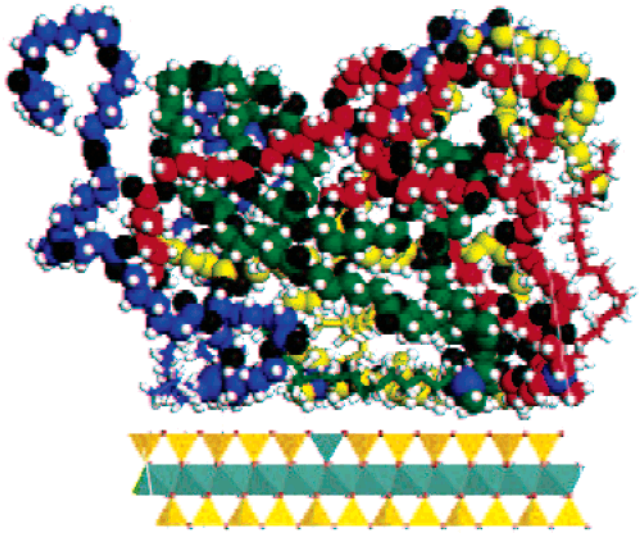

Figure 3. Snapshot of the simulations of the exfoliated PCL−Cloisite 30B nanocomposite model. The clay layer is represented by one octahedral sheet sandwiched between two tetrahedral sheets. The surfactants are represented with sticks, and the PCL chains, with spheres; the carbon atoms in the four macromolecules are in green, red, yellow, and blue, respectively, the oxygen atoms are in black, and the hydrogen atoms are in white.

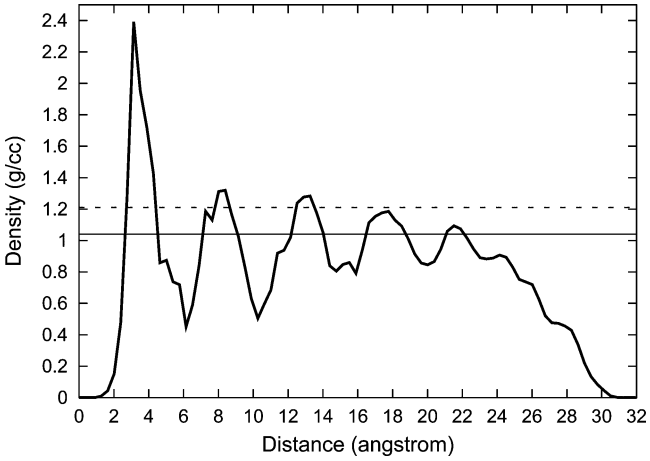

Figure 4. Density profile in the direction normal to the clay layers for the exfoliated PCL nanocomposite model (thick line). The origin of the distance axis coincides with the position of the plane of the basal oxygen atoms. Amorphous and crystalline densities for the bulk PCL are also reported (thin and dashed lines, respectively).

in the α position, as a result of the specific electronic distribution (i.e., hyperconjugation) along the methylene-ester function sequence.[38] In the snapshot of Figure 3, the PCL chains appear at first glance to be rather disordered: seven of the eight PCL octamers expand across the whole organic phase, and many of them have the central part of the chain near the outer surface while the free chain end is found inside the organic layer. The remaining oligomer (displayed in yellow) lies more or less parallel with respect to the clay surface. The density profile and the order parameter function calculated for the organic phase are discussed below; their analysis reveals that the chains are, to some extent, organized on the mmt surface.

In the density profile of the organic phase plotted in Figure 4, the origin of the distance axis is chosen to coincide with the position of the basal oxygen atoms of the surface. This profile was obtained as an average over configurations taken after the equilibration was completed and separated by 0.5 ps in time. The density distribution clearly indicates that the organic phase

is organized in successive layers. Five layers clearly appear: the first three have their maximum evenly spaced at 3.2, 8.1, and 13.0 Å from the clay surface; the fourth and fifth peaks are at 17.5 and 21.5 Å, respectively. Beyond 24 Å where the density starts to decrease, three shoulders appear at 24.3, 26.1, and 28.1 Å. It is remarkable that the maximum density of the first five peaks is higher than the density calculated for amorphous PCL under the same conditions, 1.04 g·cm^{-3}.[38] Furthermore, the maximum density of the first three peaks is higher than the experimental density for the crystalline part of PCL at 300 K, 1.21 g·cm^{-3},[50] and the maximum of the fourth peak at 17.5 Å is very close to this value (1.19 g·cm^{-3}). This long-range oscillatory profile has some implications for the traditional microscopic view of exfoliated materials, as we will see later. A very high density peak is obtained for the layer at the interface; this is indicative of the strong affinity between the polymer and the surface.[8] The adjacent peaks are lower, as a consequence of the adsorption of this first layer that partially shields the attractive potential of the clay surface. Nevertheless, the polymer chains in these farther peaks are still interacting with the surface, and this contributes,[18] along with the gradual interactions between the polymer peaks, to the formation of such layered profiles extending up to ∼2 nm from the surface. Although such simulations should ideally extend over at least 3 ns (section 2.3), we can expect these layers to remain stable upon extending the length of the simulations because all atoms remain in their equilibrium positions at this temperature. This especially concerns the layers that interact the most with the clay surface (that bears numerous negative charges), that is, up to the third or possibly fourth layer (15−20 Å). Longer simulations would also result in a smoother density profile. (A smooth aspect for the profile is not as easily obtained as for confined liquids because in this case the atoms have the additional constraint of being connected along chains that run across many adjacent organic layers.)

The order parameter P_θ defined as a function of the distance z from the basal oxygen atoms was also calculated for the chain segments

$$P_\theta(z) = \frac{3}{2}\langle \cos^2 \theta_z \rangle - \frac{1}{2}$$

where θ_z is the angle between the axis perpendicular to the clay surface (z axis) and the segment defined by the connection between atoms i and $i + 2$. The values of $\theta_z = -0.5$ and 1 correspond to chain segment orientations parallel and perpendicular to the clay surface, respectively, whereas $\theta_z = 0$ corresponds to the case where the segments are randomly oriented. The average $\langle \cos^2 \theta_z \rangle$ indicates that the values are averaged over all bonds at a given distance from the surface and over snapshots separated by 1 ps in the 200−500 ps range. The profile obtained for this function along the z direction is shown in Figure 5, along with the density profile. This profile was obtained as an average over configurations taken after the equilibration period of our selected simulations. It is remarkable that for distances up to ∼14 Å the positions of the first three density peaks coincide with the positions of the three valleys in the order parameter profile (the positions of the two maxima of the third peaks are shifted by less than 1 Å). In addition, up to 21 Å, the valleys in the density profile coincide with the peaks in the order parameter profile. These two observations lead to the following conclusions: (i) chain segments within the three high-density layers centered at 3.2, 8.1, and 13.0 Å are preferentially arranged parallel to the clay surface and (ii) segments that connect the organic layers (in regions of depleted density) are preferentially oriented perpendicular to the clay surface. At the outer surface, beyond 24 Å, the chain segments show a parallel arrangement, probably to maximize the interactions among the polymer chains.

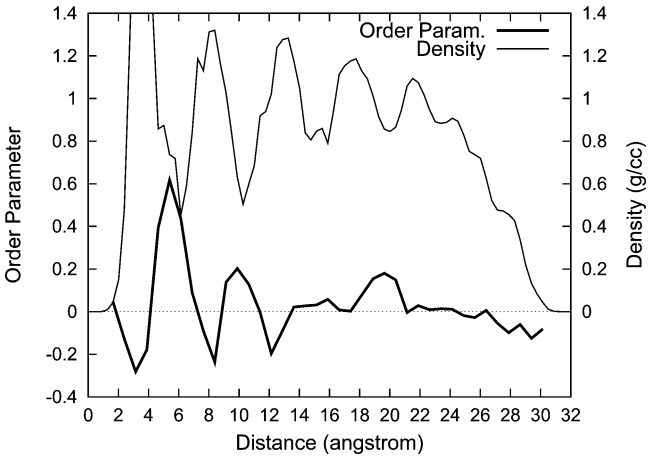

Figure 5. Order parameter for the chain segments of the organic phase as a function of the distance from the mmt surface (thick line). The density profile is also reported (thin line).

Thus for distances up to 24 Å, the organic phase shows two levels of organization: adjacent organic layers parallel to the clay surface and preferential parallel organization of the chain segments with respect to the surface within the first three layers. The range over which the preferential parallel arrangement is observed here for the polymer chain segments is slightly larger than predicted by previous simulations of generic models of polymers at interfaces. These studies, which used lattice or bead−spring models, predicted a preferential parallel alignment for the chain segments (i) in the layer closest to the surface in the case of noninteracting neutral surfaces[14,51−53] and (ii) in the first two layers in the case of strong polymer−surface interactions.[53]

The radial distribution function (RDF) has also been calculated between all carbon atoms of the organic phase (also comprising the carbon atoms of the surfactant molecules). The profile (not presented here) is very similar to the profile previously obtained for the intercalated PCL−Cloisite 25A nanocomposite.[38] Besides the expected peaks at ∼1.5, ∼2.5, ∼3.2, and ∼3.9 Å, which correspond to correlations between carbon atoms separated by one, two, and three bonds in gauche and trans conformations, respectively, a fifth peak at ∼5.0 Å is also obtained and arises from the occurrence of two successive trans conformations along a five-atom-long sequence (stretched conformations comprising dihedrals of the kinds CCCC, CCCO, or CCOC). Related to this RDF profile is thus the proportion of trans conformations: it is calculated to be in the range 64−68% for the most stable configurations obtained. This proportion is slightly higher than that obtained in the intercalated case (61−63%).

Experimentally, the gas permeability that is measured for the PCL nanocomposites is reduced with respect to the permeability measured for pure PCL or PCL-based microcomposites. A dramatic decrease in permeability is measured when a complete dispersion of the mmt platelets is achieved within the PCL matrix.[54] The gas permeability measured for a given PNC depends on the extent of clay dispersion in the polymer matrix[55] but also on the clay particle dimensions (or aspect ratios). The commonly accepted mechanism for explaining the hindered motion of gas molecules through the polymer matrix of a PNC rests on the specific arrangement of the clay platelets that creates

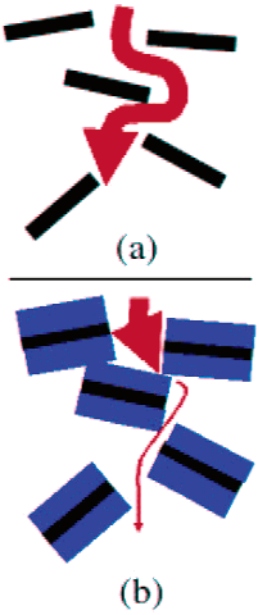

Figure 6. Schematic representation of the impeded molecular gas diffusion within a polymer nanocomposite (with gas molecule trajectories represented by the red arrows) (a) due to the tortuosity of the path only and (b) for the same platelet configuration, when the dense polymer layers are taken into account.

a tortuous path for the diffusion (see illustration in Figure 6a). The results obtained for the exfoliated nanocomposite model show a marked oscillatory density profile for distances up to ~2.4 nm from the surface, with maximum values for the density higher than in amorphous PCL. These results suggest that the successive high-density layers surrounding every dispersed platelet should also play a significant role, in addition to the mmt platelets, in impeding the diffusion of molecules within the PCL matrix. This layered arrangement of the polymer chains close to the platelets can be viewed as a "change" in the aspect ratio of the platelets, whose effective thickness is increased. The sketches in parts a and b of Figure 6 illustrate, for the same platelet configuration, the hindered motion caused by the high-density layers of polymer (part b) as opposed to the allowed motions when only bare platelets are taken into account (part a). Although Figure 6b is a 2D representation, the real system can be viewed as series of polymer "platelets" extended over each clay platelet within the polymer matrix. Experimental measurements of water diffusion into PCL−Cloisite 30B nanocomposites have established a decreasing permeability upon increasing the proportion of hydroxyl-functionalized cations (complete exfoliation is reached for a proportion of at least 50% of functionalized cations).[54] The values measured for the zero concentration diffusion coefficient D_0 are 9.76×10^{-8}, 8.43×10^{-8}, 4.07×10^{-8}, 1.24×10^{-8}, and zero cm^2/s for pure PCL and the nanocomposites organo-modified by 25, 50, 75, and 100% of functionalized cations, respectively. Hence, one can see that the D_0 values strongly decrease upon increasing the proportion of functionalized cations from 50 to 100%. Since the nanocomposite obtained is completely exfoliated in this range, this large variation in permeability measured cannot be attributed to the tortuosity of the path only. To explain the sharp decrease of D_0, the authors conjectured a combined effect of exfoliation and PCL crystallization that may lead to a "hybrid three-dimensional labyrinth".[54] The idea presented in this study that the grafted polymer chains that form high-density organic layers should play a significant role in impeding gas diffusion argues in support of their hypothesis, even though the polymer phase is found to remain amorphous.

3.2. Comparative Study of Three Nanocomposite Models. The preparation of PCL nanocomposites by melt intercalation in Cloisite 30B yields a mixed intercalated−exfoliated structure. In addition to the simulations of the model for the exfoliated PCL−Cloisite 30B nanocomposite (as obtained by in situ polymerization), the simulations of a model for the intercalated PCL−Cloisite 30B nanocomposite have been considered, and the results are discussed in this section (see the description of this model in section 2.1). For convenience, the exfoliated and intercalated models will hereafter be denoted as systems ePCL30B and iPCL30B, respectively. When using the mmt Cloisite 25A, the preparation of PCL nanocomposites also leads to a mixed intercalated−exfoliated structure, which we have modeled previously.[38] In this section, we compare the structures and energies of the two models for the PCL−Cloisite 30B nanocomposites (labeled iPCL30B and ePCL30B) and the model for the intercalated PCL−Cloisite 25A nanocomposite (iPCL25A) with an interlayer density very similar to that of the iPCL30B system (section 2.1). We will also discuss the structural factors that can drive the system toward either exfoliated or mixed intercalated−exfoliated morphology.

To compare the affinity between the three subsystems (PCL chains, surfactants, and mmt surfaces) in the various models, binding-energy values between these subsystems have been calculated. (These energies represent the negative of the interaction energies.) The energies labeled $E_{mmt-PCL}$ and $E_{mmt-surf}$ correspond to the interactions between the mmt surfaces and the polymer chains and surfactant molecules, respectively. For example, the procedure for calculating the $E_{mmt-PCL}$ binding energy starts from a minimized geometry of the complete system comprising the clay platelets, the surfactants, and the chains. The surfactant molecules are then deleted from the system. Finally, the binding energy is obtained as the energy difference between, on one hand, the sum of the potential energy of montmorillonite and the potential energy of the chains and, on the other hand, the potential energy of the interacting mmt−PCL subsystem:

$$E_{mmt-PCL} = E_{pot,mmt} + E_{pot,PCL} - E_{pot,mmt-PCL}$$

Similar procedures were followed to derive all binding energies as well as their individual van der Waals and electrostatic components. All van der Waals energies were calculated with the Lennard-Jones potential smoothly turned off over the range of 9.8−10.2 Å using a spline function to account for the interactions between the mmt surfaces and the two closest layers in the organic phase.

The final configurations obtained for the simulations of the two intercalated systems iPCL30B and iPCL25A are shown in Figure 7. Figure 8 displays the interlayer density profiles for systems iPCL25A and iPCL30B. The density profiles of the two systems show the same main features: a layered interlayer density profile (four and five peaks, respectively) with higher and sharper peaks associated with the two layers closest to the surface. Note that the heights of these higher peaks are comparable in the two systems, which suggests that similar amounts of polymer and surfactant segments are adsorbed in both cases. The various binding energies calculated for the two systems are reported in Table 2. In iPCL30B, the $E_{mmt-surf}$ and $E_{mmt-PCL}$ energies are higher by ~100 and ~30 kcal/mol, respectively, than the corresponding energies in iPCL25A. Most of the energy difference in $E_{mmt-surf}$ is due to the large difference between the respective electrostatic components, 153 kcal/mol.

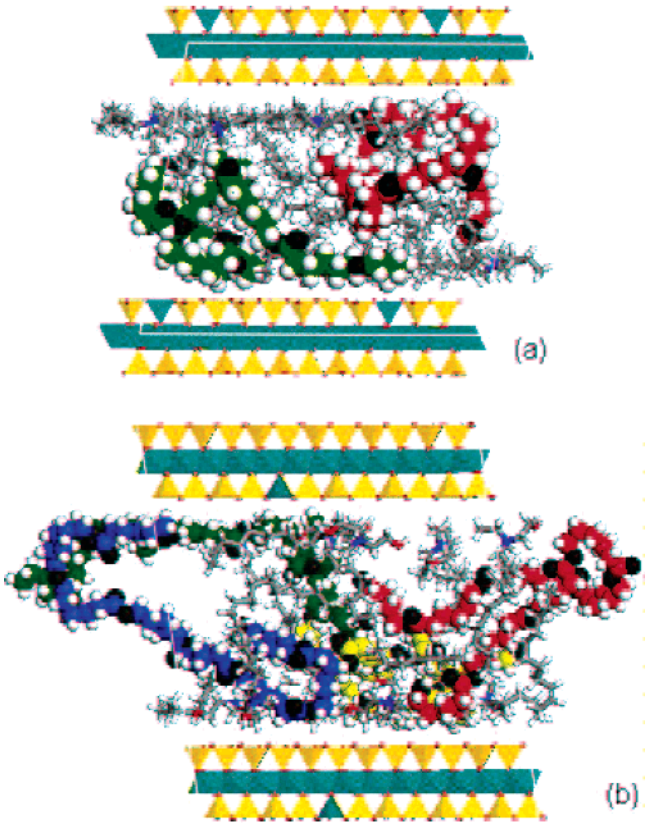

Figure 7. Snapshots of the simulations of systems (a) iPCL25A and (b) iPCL30B. In the gallery, the surfactants are represented with sticks, and the PCL chains, with spheres; the carbon atoms of the polymer chains are displayed in green, red, yellow, and blue, the oxygen atoms in black, and the hydrogen atoms in white. The snapshot for iPCL25A is taken from ref 38.

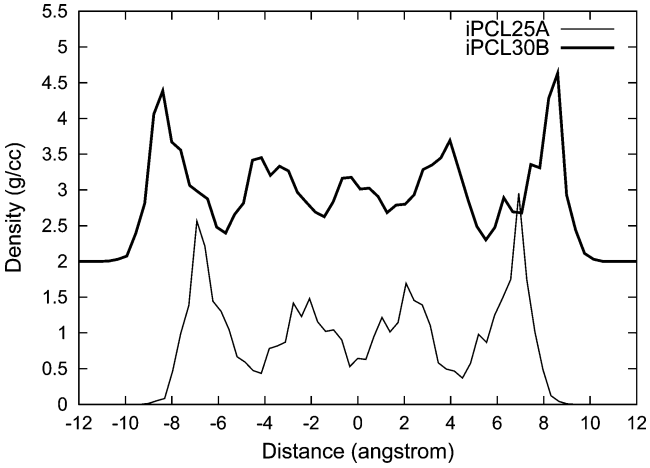

Figure 8. Density profiles of the interlayer organic phase (calculated for all of the atoms of both the polymer and surfactant chains) in the direction normal to the clay layers for the systems iPCL25A (thin line) and iPCL30B (thick line). The positions of the two planes of basal oxygen atoms are at ±10.5 and ±12.0 Å, respectively. For clarity, the profile for iPCL30B has been shifted by 2.0 along the *y* axis.

The electrostatic component of $E_{mmt-surf}$ is higher in iPCL30B because of the interactions of the charged mmt surfaces with the polar hydroxyl groups of the surfactants that remain adsorbed throughout the simulations. The van der Waals components of $E_{mmt-surf}$ and $E_{mmt-PCL}$ show opposite variations in going from system iPCL25A to system iPCL30B (−56 and +23 kcal/mol, respectively).

TABLE 2: van der Waals, Electrostatic, and Total Contributions to the Binding Energies (in kcal/mol) between the Three Subsystems PCL, Surfactants, and Montmorillonite Calculated for the Systems iPCL25A and iPCL30B[a]

		system	
		iPCL25A	iPCL30B
$E_{mmt-PCL}$	total	148 ± 12	177 ± 15
	van der Waals	95 ± 9	118 ± 19
	electrostatic	53 ± 4	59 ± 5
$E_{mmt-surf}$	total	822 ± 29	919 ± 22
	van der Waals	294 ± 16	238 ± 12
	electrostatic	528 ± 21	681 ± 10

[a] The errors bars represent ±1 standard deviation.

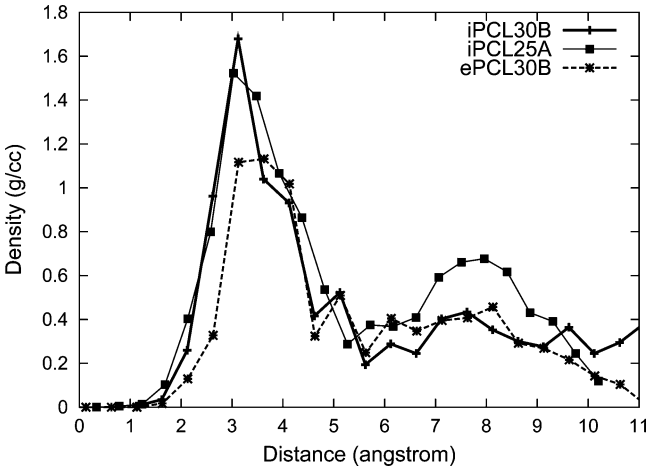

Figure 9. Partial densities of the surfactants in the first two layers next to the mmt surface calculated for systems iPCL30B, iPCL25A, and ePCL30B.

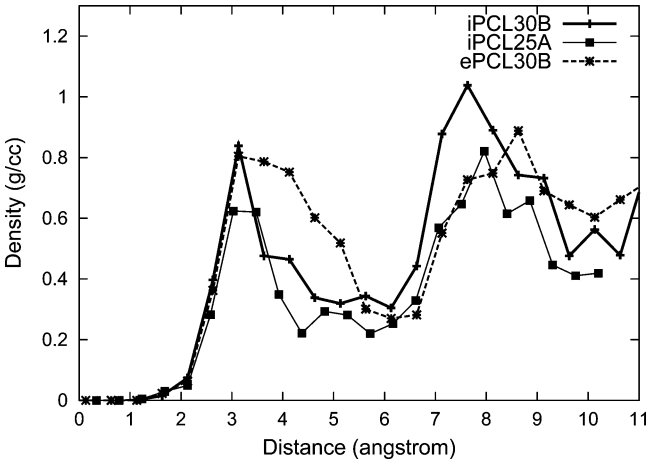

Figure 10. Partial densities of PCL in the first two layers next to the mmt surface calculated for systems iPCL30B, iPCL25A, and ePCL30B.

The chain organization at the interfaces was also examined by calculating the separate contributions to the density profiles due to the polymer and surfactant chains. These profiles displayed in Figures 9 and 10 allow us to estimate the relative amounts of polymer and surfactant in the two layers closest to the surface. The calculations of the separate profiles were made over three configurations and, for the two intercalated cases, also over the two halves of the interlayer space so as to increase the averaging. For the profiles of the surfactants in Figure 9, the two peaks closest to the surface calculated for the respective systems iPCL25A and iPCL30B have very similar height and

width. The second peak, centered at ~7.5 Å, is clearly visible in the case of system iPCL25A but is not distinguishable for iPCL30B. This reflects the spreading of the surfactant density over the three innermost layers in the latter system. For the first polymer layer in Figure 10, the peak observed for system iPCL30B is only slightly higher than the density peak of iPCL25A; both peaks appear to have a rather similar width. The second polymer peak of system iPCL30B is higher (by about 15%) and broader than that of iPCL25A. In each of the two systems iPCL25A and iPCL30B, the difference in width and height between the first and second polymer layers indicates that the polymer chains are preferentially located in the center of the gallery in these intercalated systems.

At this stage, the comparison of the results for the models iPCL25A and iPCL30B indicates a slightly higher binding interaction between the polymer and the mmt for the latter nanocomposite along with a very minor increase in the polymer density at the interface. The measurements of the rheological properties (storage and loss moduli that correspond to the elastic and plastic responses to a deformation, respectively) of pure PCL, a PCL microcomposite, and the PCL−Cloisite 25A and PCL−Cloisite 30B nanocomposites have been reported.[36] Higher moduli are measured for both nanocomposites with respect to the unfilled PCL or the microcomposite. A difference is also measured to a lesser extent for the moduli of the two nanocomposites: for the same filler content, the Cloisite 30B-based nanocomposite has the highest moduli. This difference in the experimental properties could be ascribed to the higher interactions between the PCL and the mmt in this PNC, as determined in the corresponding model (iPCL30B).

In nanocomposites, the extent of clay dispersion is thought to be related to the interfacial polymer density. Indeed, as the amount of adsorbed polymer increases, the clay platelets experience an increasing pressure exerted by the polymer chains as they try to recover their bulklike conformations and gain entropy. As a result, this is expected to yield a higher proportion of platelets that are pulled apart, ending in a larger proportion of exfoliated domains in the corresponding material. Our results indicate a slightly higher interfacial polymer density in model iPCL30B, with respect to that in model iPCL25A. This difference is due to the interactions of the polymer polar sequences CH_2-O-CO with the hydroxyl groups of the surfactants in iPCL30B. These interactions contribute to bringing the polymer chains closer to the surface, in addition to the mmt−PCL interactions found in both systems. (Evidence is provided by the binding energies calculated between the surfactants and the polymer chains, which are 377 and 464 kcal/mol in iPCL25A and iPCL30B, respectively.) Therefore, if a cause-and-effect relationship exists between a high interfacial polymer density and the dispersion of the platelets, then one would expect to reach complete exfoliation as the mmt− and surfactant−polymer interactions grow. The results obtained from experiments conducted for the PLA nanocomposites using the two mmts Cloisite 30B and Cloisite 25A are in favor of this argument. For PLA nanocomposites prepared by melt intercalation using either Cloisite 25A or Cloisite 30B, the extent of dispersion is much higher in the latter case.[56] Moreover, the preparation of the PLA nanocomposites by solution intercalation with Cloisite 30B leads to a completely exfoliated material, whereas only a mixed intercalated−exfoliated PLA nanocomposite is obtained when starting from Cloisite 25A.[57] Note that these examples also illustrate the importance of the preparation method in the final result (vide infra). The better dispersion reported for the PLA nanocomposites prepared with Cloisite 30B is thought to be the consequence of a higher interfacial polymer density; this results from significantly higher surfactant− and mmt−polymer interactions than those found in the PCL counterpart because the repeat unit of the PLA polymer is made up of the $CH(CH_3)-O-CO$ polar sequence (where hyperconjugation is also present and increases the polarity of the methine group). However, for the PCL nanocomposites prepared with Cloisite 25A and Cloisite 30B, the difference in the extent of dispersion is expected to be smaller given the small difference in interfacial polymer density found in systems iPCL25A and iPCL30B (Figure 10). The mechanical properties measured for the two PCL nanocomposites indicate only slightly higher Young's moduli and slightly lower elongations at break values for the PCL−Cloisite 30B nanocomposite for mmt contents higher than 3 wt %.[36] Therefore, because the mechanical properties improve with an increasing extent of dispersion for the PCL nanocomposites, these measurements are indicative of only a little better delamination in the case of Cloisite 30B.

In Figure 10, the peak associated with the interfacial polymer density in system ePCL30B is significantly broader than the density peak calculated for intercalated systems iPCL25A and iPCL30B. The density profiles of the surfactants in Figure 9 are consistent with these results, the lowest interfacial density being obtained for the ePCL30B system. The higher interfacial polymer density in system ePCL30B is one factor that can explain the complete dispersion in the corresponding nanocomposite. Such a high interfacial polymer density results from the preparation method (in situ polymerization) that forces the mmt−polymer contacts by creating surfactant−polymer links in the layer of the organic phase closest to the mmt surface. However, it seems that there is a minimum interfacial polymer density required for promoting the complete exfoliation. This conclusion stems from experimental data from in situ polymerizations using mixtures of nonfunctional alkylammoniums and ammoniums bearing one hydroxyl group in various ratios: a complete exfoliation is obtained when at least half of the surfactant molecules are functionalized.[54] Thus, when a sufficient number of polymer chains are grafted to the surface, we expect the resulting increase in interfacial polymer density to be the determining factor in obtaining the complete dispersion of the mmt sheets in the PCL matrix. Other experimental and theoretical findings support this conclusion:[24,58] a recent experimental study on a series of PLA-based nanocomposites prepared by melt extrusion using various surfactants shows that the extent of dispersion of the sheets is larger in the case where a chemical bond is formed between the polymer chains and the surfactants.[58] In addition, in their analytical model for the free energy of polymer melts confined between two parallel platelets, Kuznetsov and Balazs have stressed the importance of having end-functionalized chains that highly interact with the surface to promote exfoliation;[24] the highly interacting end-functionalized chains used in their model actually amount to the surfactant−polymer macromolecules in our system.

Another factor must be mentioned to explain the difference in the extent of clay dispersion in the PCL−Cloisite 30B nanocomposites prepared from the melt (mixed intercalated−exfoliated morphology) and by in situ polymerization (fully exfoliated). As we have seen, in the gallery of the iPCL25A and iPCL30B models, there is a high proportion of polymer chains adsorbed on the mmt surfaces because of favorable interactions between the mmt and polymer sequences. These interactions present a drawback: the polymer chains can also form bridging structures across the gallery by interacting with both surfaces, as revealed by the snapshot of system iPCL30B

in Figure 7 (polymer chains with carbon atoms displayed in blue and red). The formation of such bridges during the intercalation step can hinder the exfoliation process by binding the two clay surfaces.[23] In contrast, bridges are not expected to form in nanocomposites obtained by in situ intercalative polymerization. Indeed, for this preparation route, it has been established that the PCL chains start to grow from all of the functional hydroxyl groups.[37] Thus, on the basis of this result and given the high interfacial density observed in the density profile of the ePCL30B model, one can propose the following growth mechanism for the chains. In the beginning of the polymerization, the first few segments of the polymer chains will more favorably cover the surface where they are grafted (as suggested by the high density at the interface in ePCL30B); then, as the chains continue to grow, they will not be able to adsorb on the opposite surface and form bridging structures because of the covering of this surface where monomers have also undergone polymerization. Thus, the formation of these bridges appears to be inherent to the melt intercalation method and is not likely for the in situ polymerization synthetic route. This constitutes another factor that further explains the different dispersion behavior observed for the two PCL−Cloisite 30B nanocomposites.

4. Conclusions

The preparation by melt intercalation and in situ polymerization methods of poly(ϵ-caprolactone) nanocomposites using montmorillonite modified by functionalized alkylammoniums (Cloisite 30B) leads to mixed intercalated−exfoliated and exfoliated morphologies, respectively. Molecular dynamics simulations of intercalated and exfoliated models of the PCL−Cloisite 30B nanocomposites have been considered. The analysis of the structure of the exfoliated PCL nanocomposite model shows an organization of the adsorbed organic phase in adjacent layers up to 24 Å from the mmt surface. For the first four layers at distances up to 17.5 Å, the maximum densities are predicted to be higher than the density of crystalline PCL. The order parameter function was calculated to measure the chain segment orientations; the results indicate a preferential parallel organization of the polymer segments with respect to the surface in the first three layers. The long-range ordering of the organic layers leads us to propose a model for explaining the remarkable gas barrier properties of exfoliated PCL nanocomposites, which takes into account the clay platelets as well as the surrounding polymer layers with the highest densities.

The intercalated PCL−Cloisite 30B model shows a layered density profile for the organic phase in the gallery and a polymer density predominantly distributed in the second layer next to the surface. The comparison with the Cloisite 25A-based nanocomposite indicates a slightly higher interfacial polymer density along with higher mmt− and surfactant−polymer binding interactions in the PCL−Cloisite 30B nanocomposite; this can account for the differences observed in the rheological properties of these two nanocomposites. Our results also suggest a much higher interfacial polymer density for the PLA nanocomposites prepared with the same mmts. This higher interfacial density can explain the larger extent of dispersion obtained for the PLA nanocomposites (with respect to PCL), though a complete dispersion also appears to depend on the preparation method.

For the exfoliated PCL−Cloisite 30B nanocomposite, the grafting of the polymer chains to the surfaces via covalent bonding to the functionalized surfactants causes a substantial increase in polymer density in the layer at the interface (compared to that of both intercalated models), favoring platelet separation. In the intercalated nanocomposites, the polymer chains can form bridge structures across the galleries that hinder the exfoliation process, whereas such bridges are not expected to form during the in situ polymerization of the ϵ-caprolactone monomers. We believe that these structural differences come closest to explaining the difference in morphologies observed experimentally between the melt processed and the in situ polymerized nanocomposites.

Acknowledgment. We are grateful to Ph. Dubois, E. Pollet, and M. Alexandre (University of Mons-Hainaut) for many fruitful discussions. All calculations were run on an IBM eServer pSeries 655 using 16 processors and 32 GB of memory. This project is supported by the Government of the Région Wallonne, in the framework of the WDU program (TECMAVER). Research in Mons is also partly supported by the Belgian Science Policy Program (IAP Project V/3) and the Belgian National Fund for Scientific Research FNRS/FRFC.

Appendix

The charges (Table 1) derived for the dihydroxyl-bearing surfactant were obtained with the CHELPG procedure (as implemented in the Gaussian 98 package[43]), which fits the atomic charges to the electrostatic potential calculated at the HF/6-31G* level of theory. Only the charges on atoms that are around the nitrogen atom are reported. It is noteworthy that the nitrogen atom bears a low positive charge. Actually, about 70% of the excess positive charge is delocalized over the three methylene groups and the methyl group bound to the nitrogen atom (atom indices f, g, h, j, k, l, and r up to x). The charges used for the PCL chains have been reported in ref 38.

References and Notes

(1) Alexandre, M.; Dubois, P. *Mater. Sci. Eng. Res.* **2000**, *28*, 1.
(2) Bitsanis, I. A.; Pan, C. *J. Chem. Phys.* **1993**, *99*, 5520.
(3) Ballamudi, R. K.; Bitsanis, I. A. *J. Chem. Phys.* **1996**, *105*, 7774.
(4) Wang, Y.; Hill, K.; Harris, J. G. *J. Phys. Chem.* **1993**, *97*, 9013.
(5) Klatte, S. J.; Beck, T. L. *J. Phys. Chem.* **1993**, *97*, 5727.
(6) Zhan, Y.; Mattice, W. L. *Macromolecules* **1994**, *27*, 7056.
(7) Vega, L. F.; Panagiotopoulos, A. Z.; Gubbins, K. E. *Chem. Eng. Sci.* **1994**, *49*, 2921.
(8) Klatte, S. J.; Beck, T. L. *J. Phys. Chem.* **1995**, *99*, 16024.
(9) Cheng, C.; Lee, K.; Li, Y.; Wang, B. *J. Adhes. Sci. Technol.* **1998**, *12*, 695.
(10) Jin, R. Y.; Song, K.; Hase, W. L. *J. Phys. Chem. B* **2000**, *104*, 2692.
(11) Cui, S. T.; Cummings, P. T.; Cochran, H. D. *J. Chem. Phys.* **2001**, *114*, 6464.
(12) Cui, S. T.; Cummings, P. T.; Cochran, H. D. *J. Chem. Phys.* **2001**, *114*, 7189.
(13) Vacatello, M.; Yoon, D. Y.; Laskowski, B. C. *J. Chem. Phys.* **1990**, *93*, 779.
(14) Kumar, S. K.; Vacatello, M.; Yoon, D. Y. *Macromolecules* **1990**, *23*, 2189.
(15) Yoon, D. Y.; Smith, G. D.; Matsuda, T. *J. Chem. Phys.* **1993**, *98*, 10037.
(16) Smith, G. D.; Yoon, D. Y. *J. Chem. Phys.* **1994**, *100*, 649.
(17) Baschnagel, J.; Binder, K. *Macromolecules* **1995**, *28*, 6808.
(18) Jang, J. H.; Mattice, W. L. *Polymer* **1999**, *40*, 4685.
(19) Vaia, R. A.; Giannelis, E. P. *Macromolecules* **1997**, *30*, 7990.
(20) Vaia, R. A.; Giannelis, E. P. *Macromolecules* **1997**, *30*, 8000.
(21) Balazs, A. C.; Singh, C.; Zhulina, E. *Macromolecules* **1998**, *31*, 8370.
(22) Balazs, A. C.; Singh, C.; Zhulina, E.; Lyatskaya, Y. *Acc. Chem. Res.* **1999**, *8*, 651.
(23) Zhulina, E.; Singh, C.; Balazs, A. C. *Langmuir* **1999**, *15*, 3935.
(24) Kuznetsov, D. V.; Balazs, A. C. *J. Chem. Phys.* **2000**, *112*, 4365.
(25) Lee, J. Y.; Baljon, A. R. C.; Loring, R. F.; Panagiotopoulos, A. Z. *J. Chem. Phys.* **1998**, *109*, 10321.
(26) Lee, J. Y.; Baljon, A. R. C.; Loring, R. F. *J. Chem. Phys.* **1999**, *111*, 9754.

(27) Baljon, A. R. C.; Lee, J. Y.; Loring, R. F. *J. Chem. Phys.* **1999**, *111*, 9068.
(28) Zax, D. B.; Yang, D. K.; Santos, R. A.; Hegemann, H.; Giannelis, E. P.; Manias, E. *J. Chem. Phys.* **2000**, *112*, 2945.
(29) Manias, E.; Kuppa, V. *ACS Symp. Ser.* **2001**, *804*, 193.
(30) Hackett, E.; Manias, E.; Giannelis, E. P. *Chem. Mater.* **2000**, *12*, 2161.
(31) Kuppa, V.; Manias, E. *J. Chem. Phys.* **2003**, *118*, 3421.
(32) Kuppa, V.; Menakanit, S.; Krishnamoorti, R.; Manias, E. *J. Polym. Sci., Part B: Polym. Phys.* **2003**, *41*, 3285.
(33) Hackett, E.; Manias, E.; Giannelis, E. P. *J. Chem. Phys.* **1998**, *108*, 7410.
(34) Zeng, Q. H.; Yu, A. B.; Lu, G. Q.; Standish, R. K. *Chem. Mater.* **2003**, *15*, 4732.
(35) Lepoittevin, B.; Pantoustier, N.; Devalckenaere, M.; Alexandre, M.; Kubies, D.; Calberg, C.; Jérôme, R.; Dubois, P. *Macromolecules* **2002**, *35*, 8385.
(36) Lepoittevin, B.; Devalckenaere, M.; Pantoustier, N.; Alexandre, M.; Kubies, D.; Calberg, C.; Jérôme, R.; Dubois, P. *Polymer* **2002**, *43*, 4017.
(37) Viville, P.; Lazzaroni, R.; Pollet, E.; Alexandre, M.; Dubois, P. *J. Am. Chem. Soc.* **2004**, *126*, 9007.
(38) Gardebien, F.; Gaudel-Siri, A.; Brédas, J. L.; Lazzaroni, R. *J. Phys. Chem. B* **2004**, *108*, 10678.
(39) Skipper, N. T.; Chang, F. C.; Sposito, G. *Clays Clay Miner.* **1995**, *43*, 285.
(40) Accelrys, formerly Molecular Simulation Inc.: San Diego, CA; 1997.
(41) Rappe, A. K.; Casewit, C. J.; Colwell, K. S.; Goddard, W. A.; Skiff, W. M. *J. Am. Chem. Soc.* **1992**, *114*, 10024.
(42) Breneman, C. M.; Wiberg, K. B. *J. Comput. Chem.* **1990**, *11*, 361.
(43) Frisch, M. J.; Trucks, G. W.; Schlegel, H. B.; Scuseria, G. E.; Robb, M. A.; Cheeseman, J. R.; Zakrzewski, V. G.; Montgomery, J. A., Jr.; Stratmann, R. E.; Burant, J. C.; Dapprich, S.; Millam, J. M.; Daniels, A. D.; Kudin, K. N.; Strain, M. C.; Farkas, O.; Tomasi, J.; Barone, V.; Cossi, M.; Cammi, R.; Mennucci, B.; Pomelli, C.; Adamo, C.; Clifford, S.; Ochterski, J.; Petersson, G. A.; Ayala, P. Y.; Cui, Q.; Morokuma, K.; Malick, D. K.; Rabuck, A. D.; Raghavachari, K.; Foresman, J. B.; Cioslowski, J.; Ortiz, J. V.; Stefanov, B. B.; Liu, G.; Liashenko, A.; Piskorz, P.; Komaromi, I.; Gomperts, R.; Martin, R. L.; Fox, D. J.; Keith, T.; Al-Laham, M. A.; Peng, C. Y.; Nanayakkara, A.; Gonzalez, C.; Challacombe, M.; Gill, P. M. W.; Johnson, B. G.; Chen, W.; Wong, M. W.; Andres, J. L.; Head-Gordon, M.; Replogle, E. S.; Pople, J. A. *Gaussian 98*, revision A.7; Gaussian, Inc.: Pittsburgh, PA, 1998.
(44) Rappe, A. K.; Goddard, W. A. *J. Phys. Chem.* **1991**, *95*, 3358.
(45) Leach, A. R. *Molecular Modelling. Principles and Applications*, 2nd ed.; Prentice Hall: Harlow, England, 2001.
(46) Karasawa, N.; Goddard, W. A., III *J. Phys. Chem.* **1989**, *93*, 7320.
(47) Nosé, S.; Klein, M. *Mol. Phys.* **1983**, *50*, 1055.
(48) Nosé, S. *J. Chem. Phys.* **1984**, *81*, 511.
(49) Hoover, W. *Phys. Rev. A* **1985**, *31*, 1695.
(50) Perret, R.; Skoulios, A. *Die Makromol. Chem.* **1972**, *156*, 157.
(51) Theodorou, D. N. *Macromolecules* **1988**, *21*, 1400.
(52) Kumar, S. K.; Vacatello, M.; Yoon, D. Y. *J. Chem. Phys.* **1988**, *89*, 5206.
(53) Bitsanis, I.; Hadziioannou, G. *J. Chem. Phys.* **1990**, *92*, 3827.
(54) Gorrasi, G.; Tortora, M.; Vittoria, V.; Pollet, E.; Alexandre, M.; Dubois, P. *J. Polym. Sci., Part B: Polym. Phys.* **2004**, *42*, 1466.
(55) Maiti, P.; Yamada, K.; Okamoto, M.; Ueda, K.; Okamoto, K. *Chem. Mater.* **2002**, *14*, 4654.
(56) Paul, M. A.; Alexandre, M.; Degée, P.; Henrist, C.; Rulmont, A.; Dubois, P. *Polymer* **2003**, *44*, 443.
(57) Krikorian, V.; Pochan, D. J. *Chem. Mater.* **2003**, *15*, 4317.
(58) Ray, S. S.; Yamada, K.; Okamoto, M.; Fujimoto, Y.; Ogami, A.; Ueda, K. *Polymer* **2003**, *44*, 6633.